

Extreme Ultraviolet Radiation With Coherence Time Beyond 1 s

Craig Benko¹, Thomas K. Allison^{1,2}, Arman Cingöz^{1,*}, Linqiang Hua^{1,3}, François Labaye¹,
Dylan C. Yost^{1,**} & Jun Ye¹

¹*JILA, National Institute of Standards and Technology and the University of Colorado, Boulder, CO 80309-0440*

²*Stony Brook University, Departments of Chemistry and Physics, Stony Brook, NY 11794-3400*

³*State Key Laboratory of Magnetic Resonance and Atomic and Molecular Physics, Wuhan Institute of Physics and Mathematics, Chinese Academy of Sciences, Wuhan 430071, Peoples Republic of China*

Many atomic and molecular systems of fundamental interest possess resonance frequencies in the extreme ultraviolet where laser technology is limited and radiation sources have traditionally lacked long-term phase coherence. Recent breakthroughs in XUV frequency comb technology have demonstrated spectroscopy with unprecedented resolution at the MHz-level, but even higher resolutions are desired for future applications in precision measurement. By characterizing heterodyne beats between two XUV comb sources, we demonstrate the capability for sub-Hz spectral resolution. This corresponds to coherence times > 1 s at photon energies up to 20 eV, more than 6 orders of magnitude longer than previously reported. This work establishes the ability of creating highly phase stable radiation in the XUV with performance rivaling that of visible light. Further, by direct sampling of the phase of the XUV

light originating from high harmonic generation, we demonstrate precise measurements of attosecond strong-field physics.

In the infrared, visible, and near-UV spectral regions, the precision and accuracy of frequency metrology^{1,2} has vastly exceeded that of traditional spectroscopic methods. Two key enabling laser technologies driving these measurements are ultrastable lasers with long (> 1 s) coherence times^{3,4} and optical frequency combs⁵. However, for wavelengths below approximately 200 nm, conventional light sources have short coherence times⁶ and are not useful for frequency metrology. Future applications in precision measurement with highly-charged ions⁷, helium⁸, nuclear clocks⁹, or hydrogen-like and helium-like ions¹⁰ necessitate phase stable light in the XUV. The workhorse of extreme ultraviolet (XUV) and soft x-ray science, synchrotron radiation⁶, is both temporally and spatially incoherent. New free electron laser sources possess a high degree of spatial coherence but due to their single-shot nature, coherence times are never longer than their (femtosecond) pulse durations^{11–13}. Conventional XUV lasers¹⁴, based on short-lived population inversions in highly ionized pulsed plasmas, are spatially coherent but also temporally incoherent on scales useful for XUV frequency metrology.

In the last decade, high-order harmonic generation (HHG) using femtosecond lasers has emerged as method that can support both spatial and temporal coherence in XUV¹⁵ and use of HHG sources for high resolution spectroscopy in the XUV have recently been demonstrated at the MHz level^{16–19}. In this Article, we report the observation of coherence times greater than 1 second in the XUV measured via heterodyne beating between two XUV frequency comb sources based

on intracavity HHG^{20–22}. Similar to heterodyne interferometry with continuous-wave lasers, our frequency comb lasers in the near-infrared (NIR) are up-converted to the XUV and then combined to form the heterodyne beatnote. The apparatus, schematically shown in Fig.(1a), is analogous to a Mach-Zender interferometer where each arm of the interferometer contains a cavity-enhanced HHG apparatus. The first beam splitter (the acousto-optic modulator) separates the NIR frequency comb and the second beam splitter (the beam combiner, Fig. (1d)) recombines the XUV frequency combs. The heterodyne signal will provide information about the phase of the XUV light and its noise properties. We use the phase information of the heterodyne signal to probe attosecond time-scale, strong-field physics.

XUV comb generation and XUV interferometer For our experiment, we pump two independent femtosecond enhancement cavities^{20, 21, 23} (fsECs) with a high-power Yb: fiber frequency comb outputting 120 fs pulses at 154 MHz with an average power of 80 W centered at 1070 nm²⁴. To pump two fsECs, the frequency comb is split into two by an acousto-optic modulator (AOM) such that the two resulting combs have a carrier envelope offset frequency detuning of $\Delta f_{ceo} = 1$ MHz. Each fsEC (XUV1 and XUV2 of Fig. (1a)) is actively stabilized using the Pound-Drever-Hall technique with piezo-electric transducers on cavity mirrors as actuators. The carrier envelope offset is not actively stabilized, but its passive stability is sufficient for maintaining good power enhancement. Each fsEC typically operates with ~ 4.5 kilowatts of average power and peak intensity of 4×10^{13} W cm⁻². Xenon gas for HHG is injected at the cavity foci via quartz nozzles with ~ 150 μ m aperture backed by ~ 1 atmosphere of pressure. Harmonics are coupled out of the fsEC's in co-linear fashion using 330 μ m thick intracavity sapphire plates set at the Brewster angle for the fundamental

radiation to limit intracavity loss. The finesse of the fsEC was intentionally kept low to mitigate the nonlinearities of the Brewster plate and the plasma^{22,25,26}, but enhancement factors of ~ 200 were still obtained. The two XUV beams are combined (more on this below) and detected using either an electron multiplier or a photomultiplier tube (PMT) with a phosphor screen. A schematic of the optical layout is shown in Fig. (1a). Since the pump frequency combs are offset by Δf_{ceo} , the resulting XUV frequency comb will have a relative detuning of $q \times \Delta f_{ceo}$ and heterodyne beatnotes can be observed at these frequencies so that a series of beatnotes appears in the RF output of the detector, effectively mapping the XUV spectrum of the harmonics to RF domain (Fig. (1c,1e)).

Splitting the NIR frequency comb beam at the beginning of the interferometer with the AOM is straightforward, but recombination of the XUV beams at the end of the interferometer is not. Since there are no transparent materials in the XUV, there are no standard beam-splitters available for recombination. Instead, we rely on a wavefront division scheme. A silicon wafer with a $100\ \mu\text{m}$ pyramidal aperture produced by KOH etching was used as the beam combiner (Fig. (1d)). The beam from XUV2 is focused through the aperture, while the reflected beam from XUV1 is much larger than the aperture. All the optics for the XUV light, including the beam combiner, were coated with boron carbide (B_4C) to enhance their reflectivity in the XUV²⁷. In the near field, there is no overlap between the two beams, but in the far field the beams interfere with a circular, “bullseye”, fringe pattern (see Fig. (1b)). The fringe pattern can be easily observed by setting $\Delta f_{ceo} = 0$ and adjusting the relative path length of the interferometer so that pulses from XUV1 and XUV2 overlap in time at detector. To observe beat signals at finite Δf_{ceo} , the central portion of the fringe is selected with an aperture before detection. A key feature of this beam combination scheme is

that the fringe period scales weakly as $\sqrt{\lambda}$ so that the interferometer can work well over a broad range of wavelengths, allowing us to simultaneously observe beats at the fundamental, the 17th harmonic, and all the harmonics in between.

Since fsEC's XUV1 and XUV2 are both pumped by a common NIR laser, the noise in the RF beatnote is immune to the common-mode frequency noise of the Yb: fiber laser. Thus, the apparatus directly measures noise from the HHG process or the cavity-plasma dynamics²⁵. However, since the interferometer is not actively stabilized, there are small amounts of relative noise induced by vibrations in the optics, giving the two sources a non-zero relative linewidth that is technical in origin.

Phase noise measurement and demonstration of long coherence times Here we show that high harmonic generation shares many common features with classical frequency multiplication of RF signals. In frequency multiplication, the power spectral density (PSD) of the phase noise $S_\phi(f)$ increases quadratically with the harmonic order²⁸. Even if the multiplication process is noiseless, any noise around the carrier will still increase with harmonic generation, thus setting a fundamental limit of how phase noise transforms under frequency multiplication and thus the achievable coherence level in the XUV (Methods). The linewidth of a carrier can be related to $S_\phi(f)$ by the approximation²⁹,

$$1 \text{ rad}^2 \approx \int_{f_{3dB}}^{\infty} S_\phi(f) df. \quad (1)$$

The limit of the integral f_{3dB} is the point where approximately half of the power is in the carrier and half in the noise. Therefore, the 3 dB linewidth of the carrier will increase quadratically with

harmonic order. If one is not careful to have a low-noise carrier before multiplication, the carrier will start to disappear and lead to the known phenomena of carrier collapse³⁰. Fig. (2) shows the full width at half max (FWHM) of each harmonic comb tooth plotted versus harmonic order. A simple fit to $\text{FWHM} = a q^2$, where a is the scaling parameter, highlights the quadratic dependence of the linewidth. The linewidth dependence on harmonic order was also independent of intracavity power. This analysis shows that there is a fundamental scaling of phase noise from the generating laser to the resulting XUV light. For example, assuming the best available continuous wave (CW) laser with a linewidth of 30 mHz⁴, and that the fundamental comb will faithfully follow the phase of the CW laser³¹, the linewidth at the 17th harmonic would be 8.7 Hz. Fortunately for HHG, we do not observe any additional linewidth broadening mechanisms other than the unavoidable classical frequency multiplication.

We show that the previously observed linewidth originated from the differential path noise and not HHG physics so that higher levels of coherence can be observed. The differential path length noise in the interferometer can be removed by phase-stabilizing the two optical paths. A small amount of pump light leaks through the XUV optics to the detection plane which is then picked off and detected on a photodetector to provide an error signal sensitive to interferometer fluctuations. The error signal is filtered and used to apply feedback correction to the AOM frequency thus removing the relative noise (Methods). With the interferometer phase locked, we can probe any noise processes intrinsic to intracavity HHG. A dramatic change in the linewidth of the XUV beatnotes is observed with a stable interferometer. The unstabilized beatnote of the pump laser and the beatnote at the 17th harmonic are shown in Fig. (3a,3c) with the corresponding

stabilized case in Fig. (3b,3d) with a 250 mHz resolution bandwidth. Similar resolution limited beats were observed on the 3rd-19th harmonic. The coherence of the pump lasers is faithfully transferred to the harmonics as seen by the resolution-limited beatnote of 62.5 mHz in Fig. (3f). This is equivalent to a coherence time of 16 s or a stable phase relation maintained over $\sim 10^9$ consecutive pulses. This is nearly seven orders of magnitude larger coherence times than ever reported in the XUV^{16,18,32}. This establishes that our XUV comb system is extremely phase coherent and has the capability to support sub-Hz coherences in the XUV. Furthermore, we demonstrate that the common-mode noise rejection of this measurement scheme is not particularly sensitive to the two XUV comb systems being identical by also observing coherent beats from harmonics generated from Xenon gas in one cavity and Krypton in the other (Fig. 3e).

Application to attosecond strong-field physics The heterodyne beatnotes in the XUV provide unique and unprecedented access to the phase of XUV radiation. We can use this to probe attosecond physics and measure the intensity dependent dipole phase³³. This technique is a fundamentally different method for probing this phenomena than previous realizations and does not rely on extensive spatial and spectral filtering to observe interference between multiple quantum pathways^{32,34}. This technique also does not rely on referencing the short to long trajectory contributions or vice versa³⁵. It represents a complementary technique to RABBITT and related methods based on photoelectron spectroscopy³⁶⁻³⁸, which seek to determine the time-delay (or equivalently phase shift) between adjacent harmonic orders at a given intensity. In this experiment, we isolate individual harmonics and measure precisely their phase shift as a function of intensity. These phase shifts can be directly linked to temporal dynamics of the electron in the intense laser field³⁶. By putting am-

plitude modulation (AM) on one arm of the interferometer, we can measure the amount of induced phase modulation (PM) on the XUV light (Methods). For this measurement, the peak intensity of the modulated cavity was $3.4 \times 10^{13} \text{ W cm}^{-2}$ with a 15% amplitude modulation depth. The intensity dependent dipole phase can be expressed as

$$\phi = -\alpha_j \frac{U_p(I)}{\omega} = -\alpha_j \frac{I}{4\omega^3} \quad (2)$$

with I being the laser intensity, $U_p(I)$ being the pondermotive energy, ω being the laser frequency, and ϕ being the phase of the emitted XUV light. Due to our on axis spatial filtering needed to observe a high-contrast beatnote, we are primarily sensitive to the short trajectory. The schematic of the measurement is shown in Fig. (4a). The measurement required a two-step demodulation process to extract the amount of PM induced on the XUV light from the AM applied to the pump laser. Great care was taken to ensure that the amount of PM on the XUV light was not induced by parasitic PM on the pump laser (Methods). The phase of the XUV light depends on both the intensity of the light and the particular quantum path the electron traverses (Fig. (4b)). The result of the measurement is shown in Fig. (4c) where the α_j of Eq. 2 is expressed in atomic units with the convention of Yost *et al.*³². The shaded purple region corresponds to values predicted by the standard semi-classical model (SCM)³³. The grey shaded region is the range of values predicted by different approximations to below threshold harmonics³⁹.

Below-threshold, short trajectory harmonics do not originate from tunnel ionization as in the above-threshold case and are much more sensitive to the atomic potential and ionization dynamics³⁹. Our measurement is able to discriminate between contributions of the standard SCM³³ and a model that includes over-the-barrier (OTB) ionization³⁹ to confirm that the below-threshold harmonics

mostly originate from the OTB ionization. Further, our measurement for an above-threshold harmonic (15^{th} and 17^{th}) agrees well with the predictions of the SCM³³ and the below-threshold with predictions of Yost *et al.*³² and the theoretical framework of Hostetter *et al.*³⁹. Further exploration of intensity dependent phases in atoms and molecules with comparison to calculations is the subject of future work. Our phase measurement technique was able to resolve phase shifts with uncertainties at the 10^{-2} rad level, which corresponds to a time uncertainty of ~ 6 as. In contrast to typical experiments that utilize direct attosecond timing resolution³⁸, we measure the attosecond electron dynamics imprinted on the phase of the emitted XUV light originating from HHG³⁶. With system improvements, it is feasible to extend this into the ≤ 1 as regime, rivaling the highest achievable temporal resolution of attosecond electron dynamics^{36,40}. Thus, our apparatus provides direct, unambiguous access to the phase of XUV radiation and will prove to be a valuable tool for attosecond science and the dynamics of atoms and molecules in intense laser fields.

Summary and future outlook We demonstrated that HHG is extremely phase coherent. We have identified the primary noise requirements on the pump laser and shown that it is possible to support coherence times greater than 1 s in the XUV. We have also developed an interferometer capable of operating from 1070 nm - 56 nm, but with different optics and a new beam combiner⁴¹, extension to even shorter wavelengths is possible. Such an apparatus will be a vital tool for future work in dual-comb spectroscopy, Fourier transform spectroscopy⁴², high resolution molecular spectroscopy⁴³, attosecond electron dynamics in intense laser fields⁴⁴, and HHG spectroscopy⁴⁵. We have successfully probed physics at attosecond timescales using the tools of frequency metrology to measure the intensity-dependent dipole phase. Future work will require improved output coupling^{46–48} and

power-scaling^{17,49,50} schemes to extend the high level of phase coherence to shorter wavelengths possibly enabling spectroscopy of a nuclear isomer transition where highly phase-stable light will be needed for excitation.

Methods

Acousto-optic Modulator and Beat Detection. In order to create a small frequency offset between the two XUV sources, we rely on an AOM to frequency shift the pump laser such that the relative detuning is 1 MHz. Since there are no available AOMs at this frequency, we drive the AOM such that $1 \text{ MHz} = f_{rep} - f_{AOM}$. Therefore, we will observe two beats at frequencies less than f_{rep} , one at f_{AOM} and the conjugate at $f_{beat} = f_{rep} - f_{AOM}$. The conjugate beatnote is sensitive to any noise in f_{rep} . To remove this, we derive f_{AOM} by phase-locking a voltage-controlled oscillator to f_{rep} detuned by 1 MHz such that $f_{AOM} = f_{rep} - 1 \text{ MHz}$. This removes the dependence of f_{rep} from the conjugate beatnote and puts it in f_{AOM} . Therefore, the low frequency beatnote can be detected noise free where we have detectors of adequate bandwidth.

Phase Noise. A signal oscillating at a frequency ω with phase modulation can be expressed as

$$A = A_0 e^{-i\omega t - i\beta \sin(\omega_m t)} \quad (3)$$

where β is the modulation depth and ω_m is the modulation frequency. When β is small, we can express the power in the first order modulation sideband relative to the carrier by $P_{SB}/P_C = (J_1(\beta)/J_0(\beta))^2 \approx J_1(\beta)^2$, where J_n are Bessel functions. We can extend this to the case of general phase modulation and not at a particular discrete tone by $P_{SB}/P_C \approx (1/2)\Delta\phi_{rms}^2$. We can

define the phase noise power spectral density as the noise around a carrier within a bandwidth bw as

$$S_{\phi}(f) \left[\frac{\text{rad}^2}{\text{Hz}} \right] \equiv \frac{1}{2} \frac{\Delta\phi_{rms}^2(f)}{bw}. \quad (4)$$

By integrating $S_{\phi}(f)$, one arrives at Eq. 1 and gets the approximate linewidth of a signal. The f_{3dB} point is the cut-off of the integral where there is approximately half the power in the carrier and half in the noise.

Phase-Stable Interferometer. The XUV light is very sensitive to path length fluctuations and any phase fluctuations in the driving laser. Therefore, it is imperative to keep the interferometer stable in order to generate the highest levels of coherence in the XUV. The passive stability is sufficient for sub-kHz levels of coherence. To stabilize the interferometer, we use the small amount of pump laser light that co-propagates with the XUV light. Since the pump light diverges more than the XUV light, it is simple to separate it out before the detection plane. A small amount of light is picked off and sent to a photodetector where a 1 MHz beatnote is used to measure the phase fluctuations in the interferometer cause by mechanical noise on the mirrors. The beatnote is mixed with an RF synthesizer to generate an error signal. The error signal is filtered and the correction signal is applied to the 1 MHz reference frequency for the AOM. Since the fluctuations of the interferometer are small, the phase-lock loop that sets the AOM frequency can easily compensate for the small, necessary corrections.

Measurement of Intensity Dependent Dipole Phase. The intensity dependent dipole phase is expressed in Eq. 2. By trying to measure the intensity dependent phase that results from HHG, we

are effectively measuring the AM-PM coupling with the AM being on the pump laser and the PM being on the XUV light. We can mathematically describe a beatnote signal as

$$S(t) = (1 + A \sin(\Omega t + \phi_m)) \cos(\omega t + P \sin(\Omega t + \phi_m)). \quad (5)$$

ω is the frequency of the beatnote and Ω is the frequency of the applied modulation and ϕ_m is its phase. A is the amplitude modulation depth and P is the phase modulation depth. Each beatnote is characterized by its own values for A and P . To avoid confusion, the subscripts will refer to which signal it represents. For example, A_{IR} is for the amplitude modulation of pump laser and P_q is the phase modulation of the q^{th} harmonic. Our task is to determine the values for A and P at the pump and the harmonics. By taking the ratio of P_q to A_{IR} and using proper units, we can extract the intensity dependent phase coefficient α_j .

We need to extract the relevant parameters of Eq. 5 at both the harmonic of interest and the IR simultaneously. To do this, we use a two step demodulation process. By taking Eq. 5 and mixing it with a stable RF signal (LO1) at a frequency of ω and relative phase offset ϕ , we get

$$S(t) \otimes V_1 \cos(\omega t + \phi) = S_1(t) \quad (6)$$

$$S_1(t) \approx V_1 (\cos(\phi) - \frac{AP}{2} \sin(\phi) + A \cos(\phi) \sin(\Omega t + \phi_m) - P \sin(\phi) \sin(\Omega t + \phi_m)). \quad (7)$$

We have ignored terms at 2ω . We can further low pass the signals at Ω and obtain a “DC” signal

$$S_1(t) \xrightarrow{\text{Low Pass}} S_{\text{DC}} = V_1 (\cos(\phi) - \frac{AP}{2} \sin(\phi)). \quad (8)$$

Eq. 8 will be one of our primary signals. Note that the phase is set by the phase of LO1. This also assumes that the phase of the XUV beatnote is stable. This is true when we phase stabilize our interferometer.

The signal $S_1(t)$ contains terms that oscillate at the applied modulation frequency Ω . We can demodulate our signal once more using a lock-in amplifier at the correct phase ϕ_m and ignore terms at 2Ω to obtain

$$S_1(t) \otimes V_2 \sin(\Omega t + \phi_m) = S_{LIA} \approx V_1 V_2 (A \cos(\phi) - P \sin(\phi)) \quad (9)$$

S_{LIA} is our second signal. With Eq. 8, Eq. 9 and some independently measured parameters (for example, the AM-AM coupling), we can extract our parameters of interest. To measure the A_{IR} - A_q coupling, we can use our beatnote signals. Our XUV beatnotes are directly proportional to the amount of XUV power in each beam. The amount of beatnote power can also be easily measured on an RF spectrum analyzer. By changing the amount of power in one of the enhancement cavities and observing how the beatnote power changes, we can determine how much the XUV power must have changed for a given laser intensity change. A_q can be determined by

$$\Delta \text{dB} = 20 \log_{10}(1/\sqrt{x}) \quad (10)$$

$$A_q = 1 - x \quad (11)$$

with ΔdB being the measured beatnote power. By applying amplitude modulation to the pump laser on one arm of the interferometer, we can control A_{IR} very well. It is also easily measured with a photodetector. By varying the phase of LO1, we can measure S_{DC} and S_{LIA} (Eq. 8 and Eq. 9) simultaneously. With the modulation (A,P) turned off, S_{DC} tells us the phase of the beat. With the modulation on, the relative phase between S_{DC} and S_{LIA} can tell us the ratio of A/P. Since A can be measured independently, we can extract the amount of phase modulation, P. This procedure needs to be done with the IR signal and the XUV signal simultaneously to prevent any systematic errors.

The results of the measurements are shown in Fig. (4c). Each data point is the average of ~ 10 runs of data where Eq. 8 and Eq. 9 were measured while varying the phase ϕ of LO1 from 0 to 2π . The measured values for P_q were corrected for any parasitic P_{IR} by $P_q \rightarrow P_q - q \times P_{IR}$.

Signal Correction The signal correction of $P_q \rightarrow P_q - q \times P_{IR}$ is justified by experimental observations. First, the quadratic scaling of the linewidth shows that the phase of the XUV light is directly linked to the phase of the NIR light. Any phase shift $\Delta\phi$ on the NIR is $q \times \Delta\phi$ at the q^{th} harmonic. For the beatnote signals, this also implies that the phase modulation depth P_q is related to the modulation depth in the NIR by $P_q = q \times P_{IR}$. This relation is also justified by observing the beatnote signals in the presence of phase modulation on the NIR laser. By measuring the amount of phase modulation on the NIR laser and the amount induced on the XUV beatnotes via the relation of the carrier to modulation sideband heights, we have verified the relation $P_q = q \times P_{IR}$. Our lock-in detection methods also produce the same relation when additional phase modulation is placed on the NIR laser.

Modulation Effects Modulating the intensity has notable effects on the neutral/plasma density ratio inside the enhancement cavity. However, the modulation is slow at 2 kHz and the cavity feedback loop can easily follow it to maintain resonance. The effect has been previously systematically studied²⁵. Due to the neutral/plasma density changes, there is a small amount of phase modulation induced by amplitude modulation on the NIR laser. This was verified by measuring the effect with gas present and absent. This can easily corrupt the intensity dependent phase measurement and necessitates the correction described previously. Further, any cavity oscillation due to bistability²⁵ can render the signals too noisy. Therefore, by careful measurement of the phase modulation on

the NIR laser and the XUV beatnotes, we can extract the intensity dependent phase originating from HHG and not other macroscopic effects.

References

1. Udem, Th. *et al.* Optical Frequency Metrology. *Nature* 416, 233-237 (2002).
2. Bloom, B.J. *et al.* An optical lattice clock with accuracy and stability at the 10^{-18} level. *Nature* **506**, 71-75 (2014).
3. Kessler, T. *et al.* A sub-40-mHz-linewidth laser based on a Silicon single-crystal optical cavity. *Nat. Photon.* **6**, 687 (2012).
4. Bishof, M. *et al.* Optical spectrum analyzer at the atomic quantum projection noise limit. *Phys. Rev. Lett.* **111**, 093604 (2013).
5. Cundiff, S. and Ye, J. Femtosecond optical frequency combs. *Rev. Mod. Phys.* **75**, 325 (2003).
6. Attwood, D.T. *Soft X-rays and Extreme Ultraviolet Radiation*. Cambridge University Press (2007).
7. Berengut, J.C. *et al.* Electron-hole transitions in multiply charged ions for precision laser spectroscopy and searching for variations in α . *Phys. Rev. Lett.* **106**, 210802 (2011).
8. Eyler, E.E. *et al.* Prospects for precision measurements of atomic helium using direct frequency comb spectroscopy. *Eur. Phys. J. D* **48**, 43-55 (2007).

9. Campbell, C.J. *et al.* Single-ion nuclear clock for metrology at the 19th decimal place. *Phys. Rev. Lett.* **108**, 120802 (2012).
10. Herrmann, M. *et al.* Feasibility of coherent xuv spectroscopy on the 1S-2S transition in singly ionized helium. *Phys. Rev. A*, **79**, 052505 (2009).
11. Ackermann, W. *et al.* Operation of a free-electron laser from the extreme ultraviolet to the water window. *Nat. Photon.* **1**, 336-342 (2007).
12. Young, L. *et al.* Femtosecond electronic response of atoms to ultra-intense X-rays. *Nature* **466**, 5661 (2010).
13. Emma, P. *et al.* First lasing and operation of an Ångstrom-wavelength free-electron laser. *Nat. Photon.* **4**, 641-647 (2010).
14. Suckewer, S., and Skinner, C. Soft x-ray lasers and their applications. *Science* **247**, 1553 (1990).
15. Bellini, M. *et al.* Temporal coherence of ultrashort high-order harmonic pulses, *Phys. Rev. Lett.* **81**, 297 (1989).
16. Cingöz, A. *et al.* Direct frequency comb spectroscopy in the extreme ultraviolet. *Nature* **482**, 68-71 (2012).
17. Yost, D.C. *et al.* Power optimization of XUV frequency combs for spectroscopy applications. *Opt. Exp.* **19**, 23483-23493 (2011).

18. Kandula, D.Z. *et al.* Extreme ultraviolet frequency comb metrology. *Phys. Rev. Lett.* **105**, 063001 (2010).
19. Morgenweg, J. *et al.* Ramsey-comb spectroscopy with intense ultrashort laser pulses. *Nat. Phys.* **10**, 3033 (2013).
20. Jones, R.J. *et al.* Phase-coherent frequency combs in the vacuum ultraviolet via high-harmonic generation inside a femtosecond enhancement cavity. *Phys. Rev. Lett.*, **94**, 193201 (2005).
21. Gohle, C. *et al.* A frequency comb in the extreme ultraviolet. *Nature*, **436**, 234-237 (2005).
22. Mills, A *et al.* XUV frequency combs via femtosecond enhancement cavities. *J. Phys. B.* **45**, 142001 (2012).
23. Jones, R. J. and Ye, J. Femtosecond pulse amplification by coherent addition in a passive optical cavity. *Opt. Lett.* **27**, 1848 (2002).
24. Ruehl, A. *et al.* 80 W, 120 fs Yb-fiber frequency comb. *Opt. Lett.* **35**, 3015-3017 (2010).
25. Allison, T.K. *et al.* Extreme nonlinear optics in a femtosecond enhancement cavity. *Phys. Rev. Lett.* **107**, (2011).
26. Carlson, D.R. *et al.* Intracavity ionization and pulse formation in femtosecond enhancement cavities. *Opt. Lett.* , **36**, 29913 (2011).
27. Vidal-Dasilva, M. *et al.* Electron-beam deposited boron coatings for the extreme ultraviolet. *Appl. Opt.* **47**, 2926-2930 (2008).

28. Walls, F.L. and Demarchi, A. RF spectrum of a signal after frequency multiplication; measurement and comparison with a simple calculation. *IEEE Trans. on Inst. and Meas.* **24**, 210-217 (1975).
29. Hall, J.L. An introduction to phase-stable optical sources. (Proceedings of the International School of Physics-Enrico Fermi, edited by E. Arimondo, WD Phillips, and F. Strumia (North-Holland), 1992).
30. Telle, H.R. Absolute measurement of optical frequencies. *Frequency control of semiconductor lasers* Wiley, New York (1996).
31. Schibli, T. R. *et al.* Optical frequency comb with sub-millihertz linewidth and more than 10 W average power. *Nat. Photon.* **2**, 355359 (2008).
32. Yost, D.C. *et al.* Vacuum-ultraviolet frequency combs from below-threshold harmonics. *Nat. Phys.* **5**, 815-820 (2009).
33. Lewenstein, M. *et al.* Phase of the atomic polarization in high-order harmonic generation. *Phys. Rev. A*, **52**, 4747-4754 (1995).
34. Zaïr, A. *et al.* Quantum path interferences in high-order harmonic generation. *Phys. Rev. Lett.*, **100**, 143902 (2008).
35. Corsi, C. *et al.* Direct interferometric measurement of the atomic dipole phase in high-order harmonic generation. *Phys. Rev. Lett.*, **97**, 023901 (2006).

36. Mairesse, Y. *et al.* Attosecond synchronization of high-harmonic soft x-rays. *Science*, **302**, 15403 (2003).
37. Sansone, G. *et al.* Measurement of harmonic phase differences by interference of attosecond light pulses. *Phys. Rev. Lett.* **94**, 193903 (2005).
38. Chang, Z. *Fundamentals of Attosecond Optics*. CRC Press, Boca Raton, Florida, first edition (2011).
39. Hostetter, J. *et al.* Semiclassical approaches to below-threshold harmonics. *Phys. Rev. A*, **82**, 23401 (2010).
40. Krausz, F. and Ivanov, M. Attosecond physics. *Rev. Mod. Phys.* **81**, 163-234 (2009).
41. Agåker, M. *et al.* Novel instruments for ultra-soft X-ray emission spectroscopy. *Nuc. Inst. and Meth. A*, **601**, 213219 (2009).
42. F. Keilmann *et al.*, Time-domain mid-infrared frequency-comb spectrometer. *Opt. Lett.* **29**, 1542 (2004).
43. Hinnen, P. *et al.* XUV-laser spectroscopy of HD at 92-98 nm. *Phys. Rev. A*, **52**, 4425 (1995).
44. Shafir, D. *et al.* Resolving the time when an electron exits a tunneling barrier. *Nature*, **485**, 343346 (2013).
45. Itatani, J. *et al.* Tomographic imaging of molecular orbitals. *Nature* **432**, 867-871 (2004).
46. Moll, *et al.* Output coupling methods for cavity-based high-harmonic generation. *Opt. Exp.* **14**, 81898197 (2006).

47. Pupeza, I. *et al.* Compact high-repetition-rate source of coherent 100 eV radiation. *Nat. Photon.* **7**, 608-612 (2013).
48. Yost, D.C. *et al.* Efficient output coupling of intracavity high-harmonic generation. *Opt. Lett.* **33**, 1099101 (2008).
49. Lee, J. *et al.* Optimizing intracavity high harmonic generation for XUV fs frequency combs. *Opt. Express* **19**, 2331523326 (2011).
50. Carstens, H. *et al.* Megawatt-scale average-power ultrashort pulses in an enhancement cavity. *Opt. Lett.* **39**, 2595 (2014).

Acknowledgements We acknowledge technical contributions and collaborations from Axel Ruehl, Ingmar Hartl, and Martin Ferrman. This work is supported by NIST, AFOSR, and the NSF Physics Frontier Center at JILA.

Competing Interests The authors declare that they have no competing financial interests.

Correspondence Correspondence and requests for materials should be addressed to J.Y. (email: ye@jila.colorado.edu) or C.B. (email: craig.benko@colorado.edu).

* Current Address: AOSense, Sunnyvale, CA 94085-2909

** Current Address: Max-Planck-Institut für Quantenoptik, Hans-Kopfermann-Str. 1, 85748 Garching, Germany

Author contributions All of the authors contributed to the design and performed the experiment. All of the authors discussed the results and contributed to the final manuscript.

Fig. 1

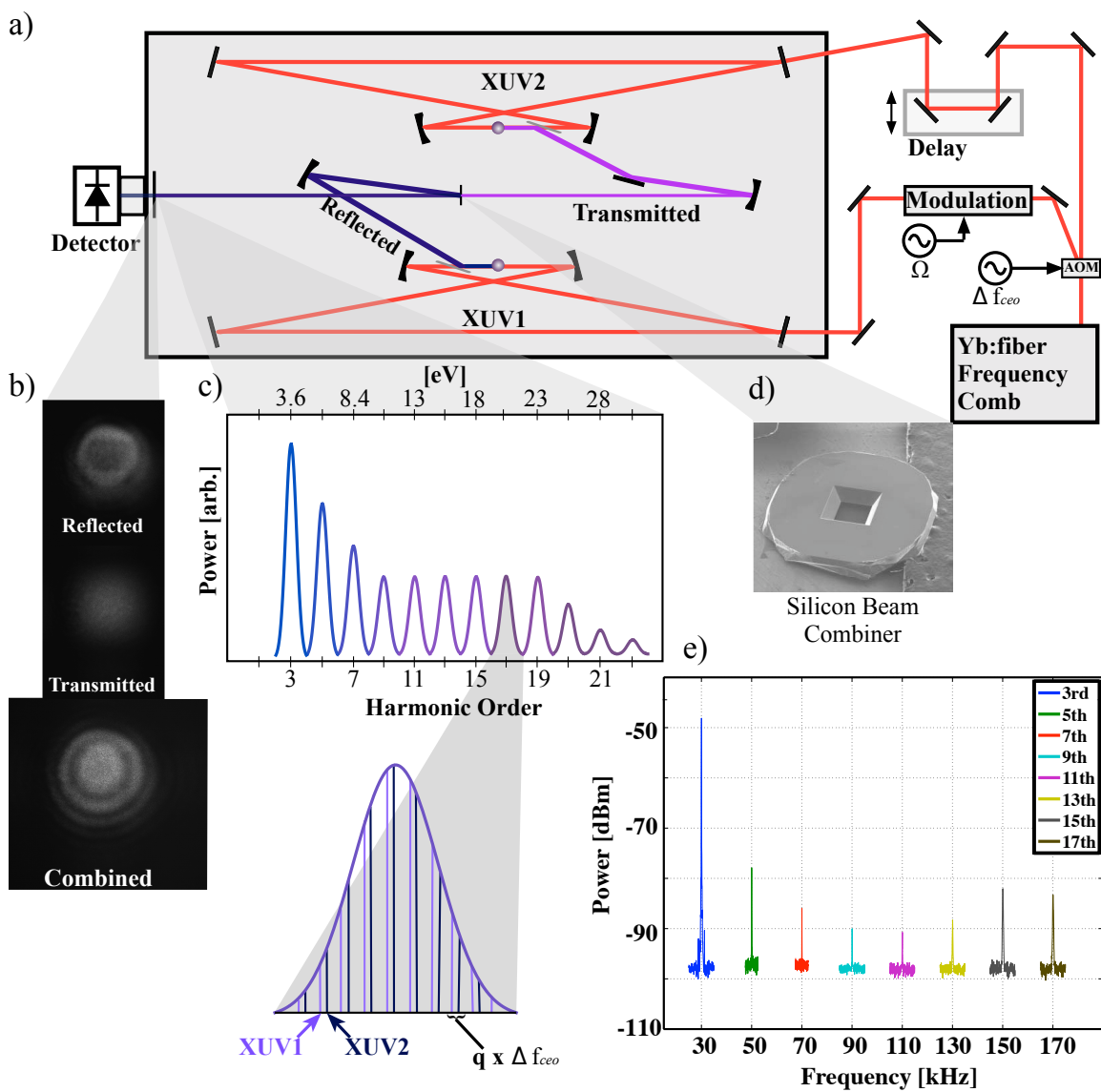


Fig. 2

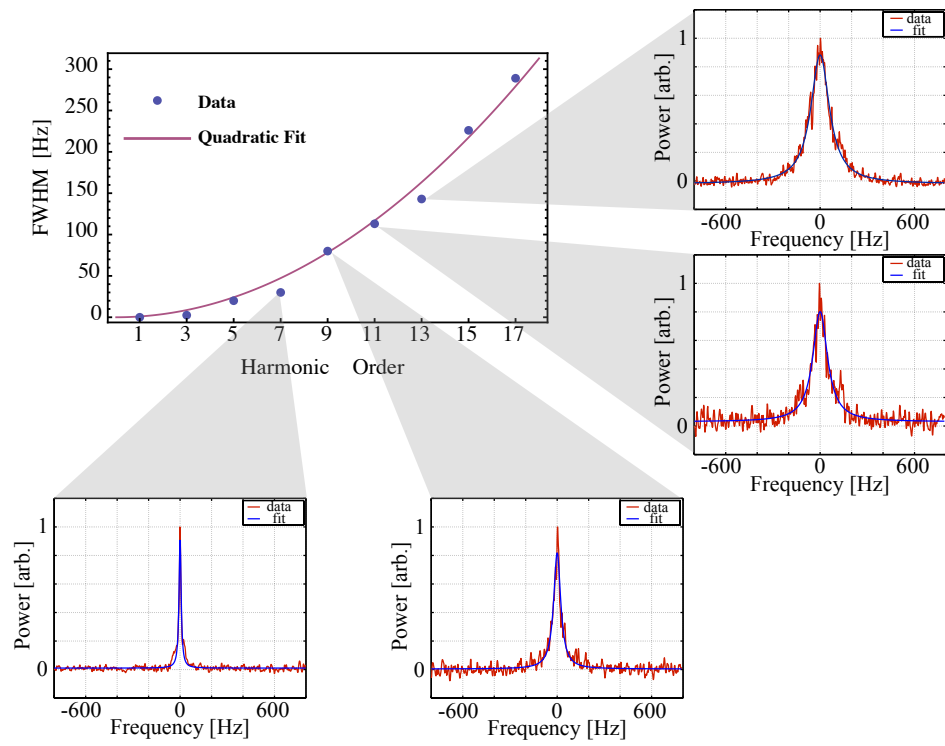


Fig. 3

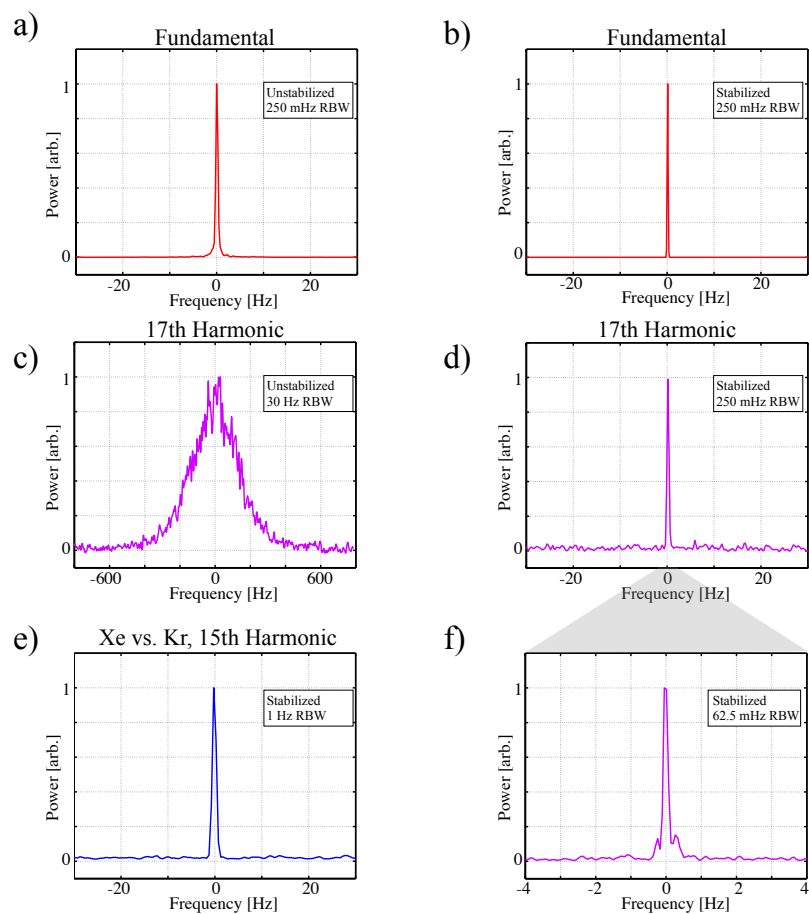


Fig. 4

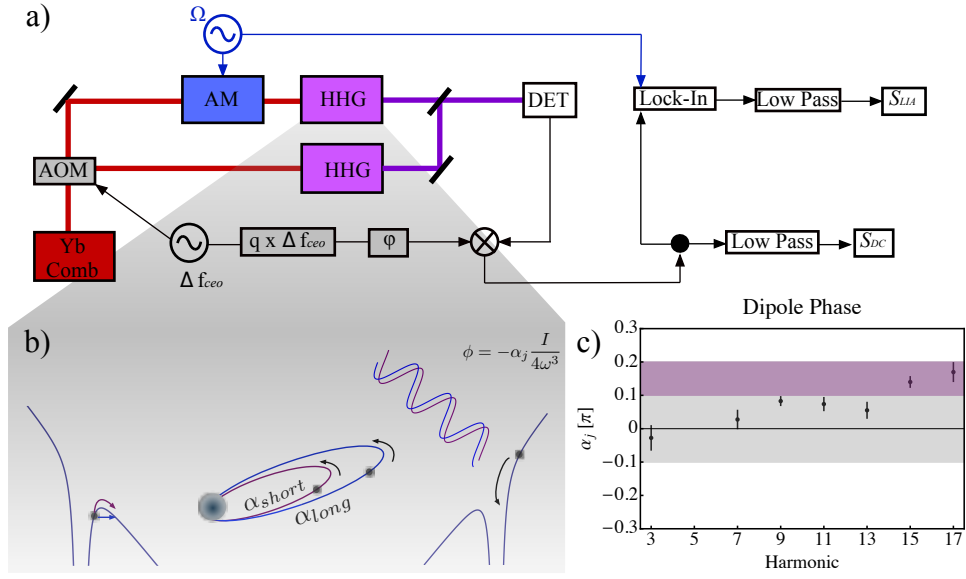


Figure 1 Schematic of the experiment and harmonic spectra. **a)** A high-powered frequency comb is split with an acousto-optic modulator (AOM) to create a f_{ceo} shift of 1 MHz. The split beams are then coupled into independent femtosecond enhancement cavities (XUV1, XUV2) to reach intensities suitable for high harmonic generation. The harmonic light is outcoupled with a Brewster plate and is steered to the beam combiner (shown in **d**)) with XUV optics. **b)** Transmitted, reflected, and combined beam profiles. The central interference fringe is selected with a spatial filter before detection. **c)** A schematic of a the harmonic spectrum. Each harmonic order has frequency comb structure with teeth spaced by the laser repetition rate. **e)** The measured radio-frequency beatnotes of the 3rd-17th harmonic. The beatnotes were mixed down to lower frequencies from $q \times 1$ MHz for clarity. The beatnotes are shown on a 30 Hz resolution bandwidth.

Figure 2 Linewidth scaling of comb teeth versus harmonic order. The fullwidth half max of the harmonic beatnotes are plotted versus harmonic order. A clear quadratic dependence is shown by the fit.

Figure 3 Demonstration of sub-Hz coherence in the XUV. **a,c)** Unstabilized beatnotes of the pump laser and the 17th harmonic. **b,d)** Stabilized beatnotes of the pump laser and the 17th harmonic. **f)** The resolution of the 17th harmonic can further be improved to a 62.5 mHz resolution bandwidth limited showing a coherence time of > 16 s. **e)** The comparison of the two sources when one is injected with Krypton and the other with Xenon. A 1 Hz resolution bandwidth limited signal is achieved.

Figure 4 Measurement of the intensity dependent dipole phase. **a)** A schematic of the signal pathway. A two step demodulation process is necessary to detect the phase modulation on the XUV light induce by amplitude modulation on the pump laser. **b)** After an electron is ionized, it accelerates in the electric field. Two dominant quantum trajectories (short and long) are important for the XUV emission where the phase of the light depends directly on the intensity of the electric field and its quantum path. **c)** Intensity dependent phase of the atomic dipole for the “short” trajectory of the 3rd-17th harmonic. The grey area is the predicted region where the below-threshold harmonic intensity dependent phase can fall. The purple shaded region is where the above-threshold intensity dependent phase is predicted to lie.